Quantum Electronics **49** (7) 641–648 (2019)

LASERS

https://doi.org/10.1070/QEL16913

Thermoelectrically cooled, repetitively pulsed Fe:ZnSe laser

N.G. Zakharov, A.V. Zakhryapa, V.I. Kozlovsky, Yu.V. Korostelin,
Ya.K. Skasyrsky, M.P. Frolov, R.S. Chuvatkin, I.M. Yutkin

Abstract. **We report the investigation of a repetitively pulsed laser based on a Fe:ZnSe crystal, cooled to a temperature of 195 K by two thermoelectric modules with a maximum cooling power of 34 W. Two pulsed synchronised Er:YAG lasers, operating in the free-lasing regime, are used for pumping. It is shown that the average laser power in a series of short pulses may exceed 20 W. An average power of 3.1 W is attained in the stationary temperature regime. The lasing spectrum is centred at a wavelength of 4.38 μm, and the total divergence angle is 5 mrad.**

Keywords: *mid-IR range, II–VI crystals, Fe:ZnSe laser, thermoelectric cooling, repetitively pulsed regime.*

1. Introduction

II-VI compounds doped with divalent chromium and iron ions have been actively studied for 20 years as promising laser media operating in a spectral range of 2–7 μm. Many of recent studies have been devoted to the application of lasers of this type for implementing highly sensitive methods of spectral analysis [1–8], in ultrahigh-resolution spectroscopy [9–11], and in design of IR femtosecond sources [12–18].

Much attention is also paid to the development of high-power pulsed lasers based on Fe:ZnSe crystals for a spectral range of 3.8–5 μm, which spans the atmospheric transparency window. The best results have been obtained for the active element cooled by liquid nitrogen: the maximum output energy of a Fe:ZnSe laser in the single-pulse regime reached 10.6 J [19]. An average output power of 35 W was demonstrated in the repetitively pulsed regime (at a pulse repetition rate of 100 Hz) [20]. In both cases pumping was performed by Er:YAG lasers with $\lambda = 2.94$ μm and a pulse width of several hundreds of microseconds.

A necessary condition for efficient laser operation at room temperature is the use of short pump pulses, because the internal quantum efficiency of laser transition decreases with increasing temperature as a result of activation of multiphonon nonradiative recombination. For example, under pumping by 250-ns pulses from a HF laser, the output energy of the Fe:ZnSe laser at room temperature reached 1.67 J [21].

The main problem in scaling room-temperature Fe:ZnSe lasers is the absence of appropriate pump sources generating high-power short pulses in the vicinity of $\lambda = 3$ μm. In addition, the increase in the pump power due to the pulse shortening is limited by the crystal radiation resistance. At the same time, liquid-nitrogen-cooled Fe:ZnSe lasers, which demonstrated the best energy characteristics, are inconvenient for practical use.

In this context, it is of interest to develop thermoelectrically cooled Fe:ZnSe lasers. This approach, applied for the first time in [22], made it possible then to implement single-pulse lasing in the vicinity of $\lambda = 4.3$ μm with an output energy of 7.5 J for a Fe:ZnSe crystal cooled to 220 K using a three-stage thermoelectric module [23]. The purpose of our work was to investigate the repetitively pulsed regime of a thermoelectrically cooled Fe:ZnSe laser and the possibility of obtaining an average power of several watts.

2. Experimental setup

A schematic of the experimental setup is presented in Fig. 1a. We used two active elements of the Fe:ZnSe laser, which were made of two different single crystals grown on a crystalline seed by physical transport in helium [24]. One of them (element 1) was a parallelepiped with an active length of 17 mm (along the cavity axis) and had transverse sizes of 25 × 25 mm. The other (element 2) was a cylinder with an active length of 19.6 mm and a diameter of 12 mm. The transmission spectra of these elements are presented in Fig. 2.

The operating faces of active elements, which were not made antireflective, were parallel with a deviation angle no larger than 30″. The active element was placed in a vacuum chamber. Element 1 was clamped via indium gaskets from two opposite sides by two four-cascade thermoelectric modules TB-4-(199-97-49-17)-1.5 (Kryotherm), soldered to water-cooled copper heat sinks (Fig. 1b). Element 2 was placed in a copper cube with sizes of 22 × 22 × 22 mm using a collet chuck, via an indium gasket. The cube was clamped via indium gaskets from two opposite sides by two four-cascade thermoelectric modules. The plane-parallel CaF_2 windows of the vacuum chamber and the active-element operating surfaces were oriented perpendicular to the cavity optical axis.

The active-element temperature was measured by a copper–constantan thermocouple. One contact of the thermocouple was fixed on the copper heat sink, and the other was fixed in the indium gasket between the crystal (shaped as a

N.G. Zakharov, A.V. Zakhryapa, R.S. Chuvatkin, I.M. Yutkin Russian Federal Nuclear Center 'All-Russian Research Institute of Experimental Physics', prosp. Mira 37, 607190 Sarov, Nizhny Novgorod region, Russia; e-mail: Nikitagz@rambler.ru, a.zakhryapa@gmail.com, rinatch@yandex.ru, yutkin@otd13.vniief.ru;
V.I. Kozlovsky P.N. Lebedev Physical Institute, Russian Academy of Sciences, Leninsky prosp. 53, 119991 Moscow, Russia; National Research Nuclear University 'MEPhI', Kashirskoe shosse 31, 115409 Moscow, Russia; e-mail: kozlovskiyvi@lebedev.ru;
Yu.V. Korostelin, Ya.K. Skasyrsky, M.P. Frolov P.N. Lebedev Physical Institute, Russian Academy of Sciences, Leninsky prosp. 53, 119991 Moscow, Russia; e-mail: yukor@x4u.lebedev.ru, yans@sci.lebedev.ru, frolovmp@sgi.lebedev.ru

Received 20 November 2018; revision received 23 January 2019
Kvantovaya Elektronika **49** (7) 641–648 (2019)
Translated by Yu.P. Sin'kov

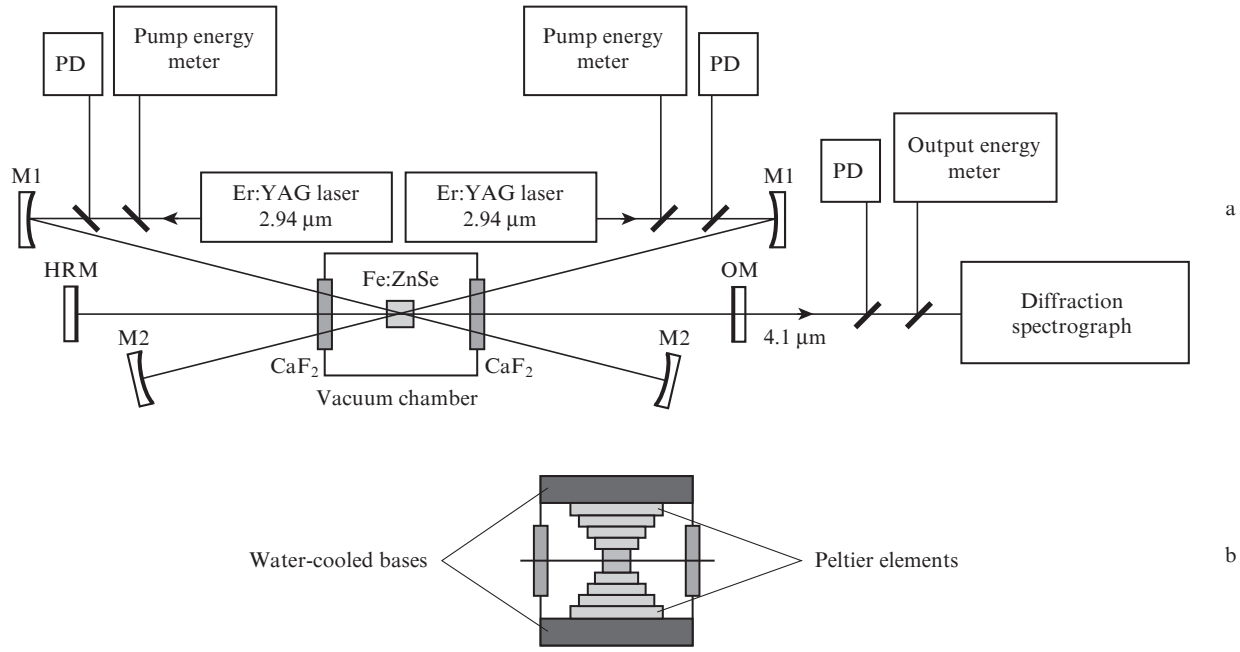

Figure 1. (a) Schematic of the experimental setup: (HRM, OM) highly reflecting and output mirrors of the Fe:ZnSe laser cavity, respectively; (CaF_2) vacuum chamber windows; (M1) mirrors directing the Er:YAG laser pump beams into the Fe:ZnSe crystal; (M2) mirrors restoring the pump radiation reflected by the faces of the Fe:ZnSe crystal and transmitted through it into this crystal; (PD) photodiodes. (b) Vacuum chamber (side view).

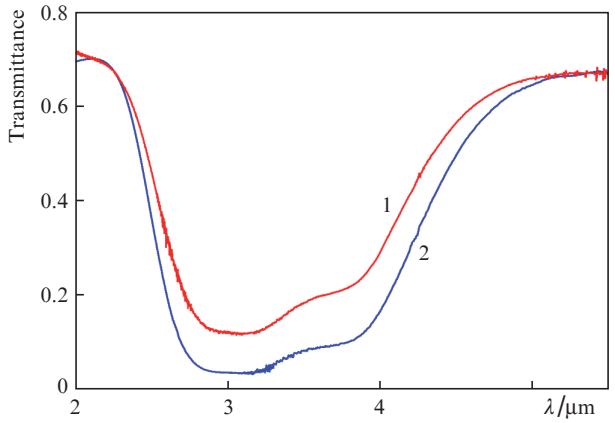

Figure 2. Transmission spectra of active elements 1 and 2 of the Fe:ZnSe laser.

parallelepiped) and the 'cold' surface of the thermoelectric module or in the copper cube (when using a cylindrical active element). A typical dependence of the heat power Q that can be withdrawn by one thermoelectric module from the 'cold' surface on the temperature difference ΔT between the 'cold' and 'hot' surfaces (referred to below as the temperature difference on a thermoelectric module) is presented in Fig. 3.

The solid line in Fig. 3 corresponds to manufacturer's data; the maximum drop and power values are given with an error of 10%. The maximum temperature difference in our experimental setup was 100 K ± 2 K. On the assumption that the maximum cold-productivity Q_{max} remains the same, the corresponding dependence somewhat changes (dashed line).

The Fe:ZnSe crystal was pumped by beams ($\lambda = 2.94$ μm) of two identical lamp-pumped pulsed Er:YAG lasers operating in the free-lasing regime. The sync pulse of the power supply of one of the lasers initiated a discharge in the other laser. Experiments were performed with discharge pulse widths $\tau = 350$ or 700 μs for each pump lamp. The power supplies of Er:YAG lasers provided a pulse repetition rate up to 20 Hz. Figure 4 shows oscillograms of lasing pulses of two pump lasers at $\tau = 700$ μs. It can be seen that the lasing in the Er:YAG laser in the second half of the pump pulse has a more pronounced spike character. A typical spike width is 1 μs.

In the single-pulse regime the maximum total energy of two Er:YAG lasers was 12 J. In the multipulse regime a change in the pulse energy was observed, especially during the first 2 s (see Fig. 5).

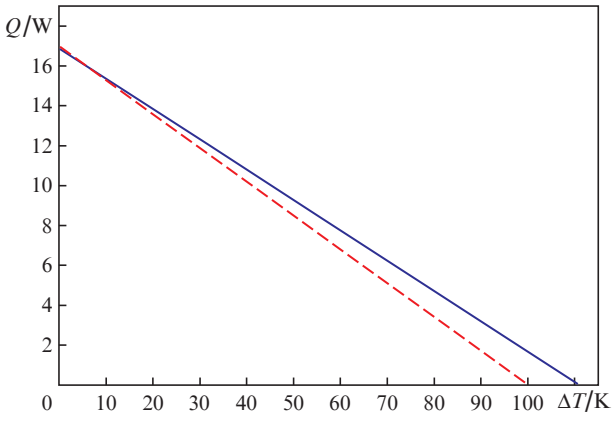

Figure 3. Dependence of the cooling power of thermoelectric module on the temperature difference across it according to manufacturer's data (solid line) and a similar dependence with correction of the maximum attainable difference based on the measurement results (dashed line).

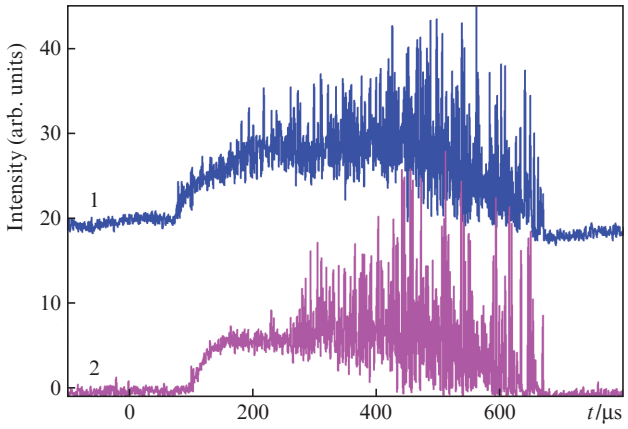

Figure 4. Oscillograms of lasing pulses of two Er:YAG pump lasers.

At low frequencies (1–4 Hz, Fig. 5a) the pulse energy of the Er:YAG laser increases during the first second. At high frequencies (8–10 Hz, Fig. 5b), after a small rise in the pulse energy, one can observe its drop during ~1.5 s. In both cases a rapid change in the average power occurs for 1–2 s. The further change in the pump power is much smaller than the observed change in the average value of the Fe:ZnSe laser power. The difference in the behaviour of the pump laser power at different repetition rate but approximately the same average lamp pump power is apparently related to the formation of different thermooptical lenses in the Er:YAG rod, which affect the Q factor of the Er:YAG laser cavity.

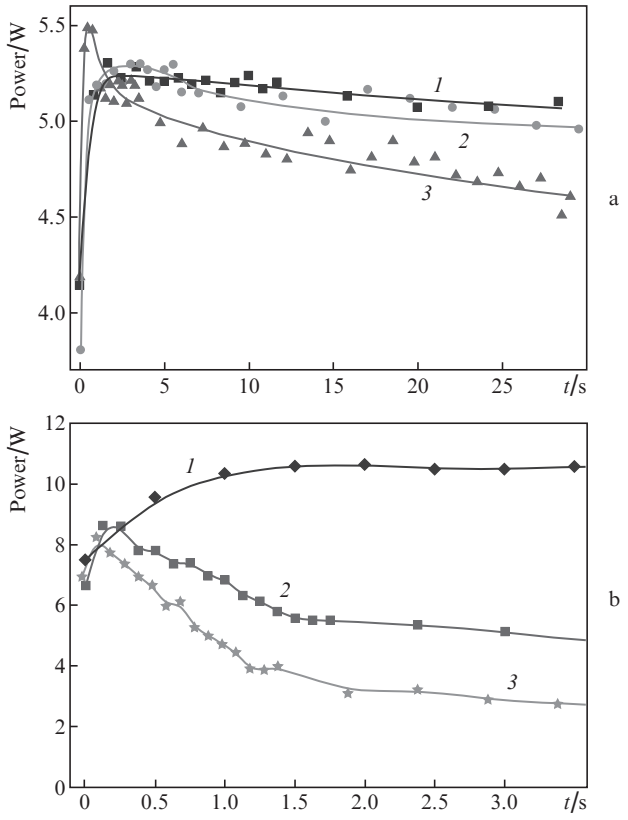

Figure 5. Temporal change in the average power of one Er:YAG laser at initial average powers of (a) ~4 W and (b) ~7 W and pulse repetition rates of (*1*) 1.2, (*2*) 2, and (*3*) 4 Hz (a) and (*1*) 2, (*2*) 8, and (*3*) 10 Hz (b).

The beams of pump lasers were introduced into the Fe:YAG crystal at a small (~4°) angle with respect to the cavity axis from two opposite sides. Under these conditions, the output end faces of Er:YAG laser rods 4 mm in diameter were imaged [with the aid of spherical mirrors M1 (R = 300 mm)] on the end faces of the Fe:ZnSe crystal with a magnification of 2:1 in the form of spots 8 mm in diameter. To use more efficiently the Er:YAG pump beams, they were returned (after the reflection from the faces of the Fe:ZnSe crystal and transmission through it) to the active region of the Fe:ZnSe laser by spherical mirrors M2 (R = 300 mm), located at distances of 300 mm from the Fe:ZnSe crystal.

The 80-cm-long cavity of the Fe:ZnSe laser was formed by a nonselective spherical highly reflecting mirror (HRM) with a curvature radius of 2 m and a flat output mirror (OM) with a reflectance of 25% in the spectral range of 4.0–4.5 μm.

The energies of pump and lasing pulses were measured using OPHIR calorimeters, and the pulse shapes were recorded, respectively, by PD-36 and PD-48 photodiodes (IBSG Co, Ltd). The lasing spectrum was measured by a spectrograph with a diffraction grating of 300 lines mm^{-1}, operating in the first order in the spectral range of 4–4.5 μm. The spectrum was recorded from a thermal print on thermal fax paper, located in the cassette part of the spectrograph. The laser beam divergence was determined by measuring the fraction of the pulse energy transmitted through a set of diaphragms positioned in the focal plane of the spherical mirror with a focal length of 500 mm.

3. Experimental results

3.1. Laser characteristics in the single pump regime

Figure 6 shows the dependence of the output energy E_{las} of the Fe:ZnSe laser on the total pump energy E_p, obtained for the laser with active element 1 in the regime of single 700-μs pump pulses. The pump pulse threshold energy was 0.67 J. At the maximum pump pulse energy (12 J), the output energy of the Fe:YAG laser was 4.1 J. The differential laser efficiency was determined from the slope of the straight line plotted based on experimental points to be 36%, which is in good agreement with the results of [23]. Approximately the same value was obtained using active element 2.

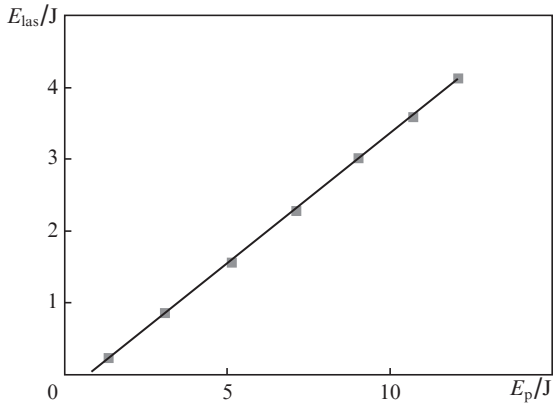

Figure 6. Dependence of the output energy of Fe:ZnSe laser on the total pump pulse energy.

The dependences of the single-pulse energy for the Fe:ZnSe laser with active element 1 on the temperature difference ΔT at two pump pulse energies are presented in Fig. 7. The temperature of the water cooling the copper heat sink was 17 °C. The difference between the temperatures of the water and the 'hot' surface of the thermoelectric module did not exceed 5 K. In the case of a single pump pulse, the difference between the temperatures of the crystal and the 'cold' thermoelectric module surface was negligible; therefore, the crystal temperature T at $\Delta T = 100$ K was assumed to be 195 K.

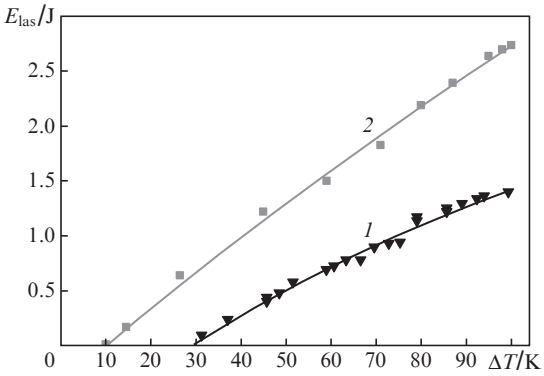

Figure 7. Dependences of the pulse energy for a Fe:ZnSe laser with active element 1 on ΔT at pump pulse energies of (*1*) 4.5 and (*2*) 8 J.

The decrease in the laser pulse energy with a decrease in ΔT is due to the rise in the lasing threshold upon crystal heating because of the shortening of the upper level lifetime for the Fe:ZnSe laser. It can be seen in Fig. 7 that an increase in the pump pulse energy provides a wider temperature range of laser operation.

Figure 8a shows the oscillograms of Fe:ZnSe laser pulses at different ΔT values and E_p = 4.5 J; for comparison, oscillograms recorded at different E_p values and ΔT = 97 K are presented in Fig. 8b. Zero on the time axis corresponds to the discharge onset in the pump laser lamps. It can be seen that, with an increase in the crystal temperature (i.e., decrease in ΔT) the instant of lasing pulse termination shifts to the pump

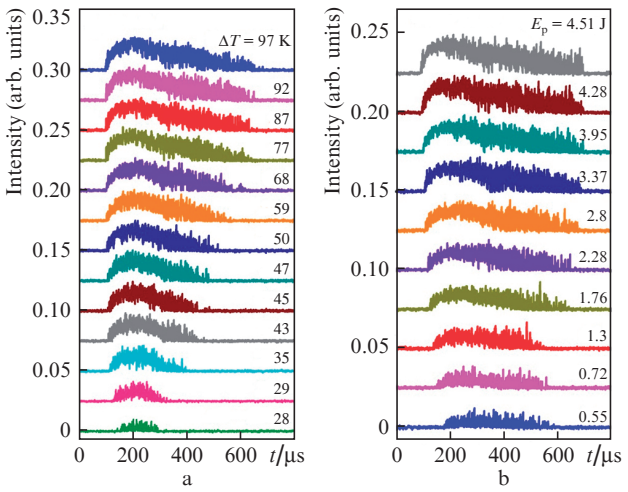

Figure 8. Oscillograms of Fe:ZnSe laser pulses (a) at different ΔT values and E_p = 4.5 J and (b) at different energies E_p and ΔT = 97 K.

pulse onset. A decrease in the pump pulse energy causes a smaller shift. This difference is explained as follows: with a change in ΔT from 100 to 30 K (corresponding to the change in the crystal temperature from 195 to 265 K), the lifetime of the upper laser level decreases from ~ 15 to 1 μs and becomes comparable with the width of pump pulse spikes. Indeed, the energy threshold in the pulsed regime is given by the formula [25]

$$E_{th} = E_0 \frac{\tau_s/\tau}{1 - e^{-\tau_s/\tau}}, \quad (1)$$

where τ is the lifetime of the upper laser level, E_0 is the threshold energy at $\tau^{-1} = 0$, and τ_s is the spike width. Let us now compare the lower oscillograms in Figs 8a and 8b, corresponding to lasing at a small excess above the threshold. As was noted above, the spike character of pumping becomes more pronounced in the second half of the pulse and develops to its end. In the case of ΔT = 28 K and E_p = 4.5 J, when $\tau \approx \tau_s$, the threshold increases by a factor of 1.6 by the end of the pulse. Therefore, heating the crystal leads to suppression of lasing in the second part of the pulse, whereas at ΔT = 97 K and E_p = 0.55 J, when $\tau \gg \tau_s$, the threshold remains constant during the pulse. In the repetitively pulsed regime, one can obtain a higher average laser power by decreasing the pulse width.

Figure 9a shows the lasing spectra of the Fe:ZnSe laser for two different active elements and different ΔT values. It can be seen that the lasing spectrum obtained using active element 2, which is characterised by higher absorption of pump radiation per pass as compared with element 1 (see Fig. 2), is red-shifted in the case of ΔT = 100 K. The dip in the spectra in the vicinity of 4.2–4.3 μm is due to the intracavity absorption of radiation by the CO_2 molecules present in the air. Upon

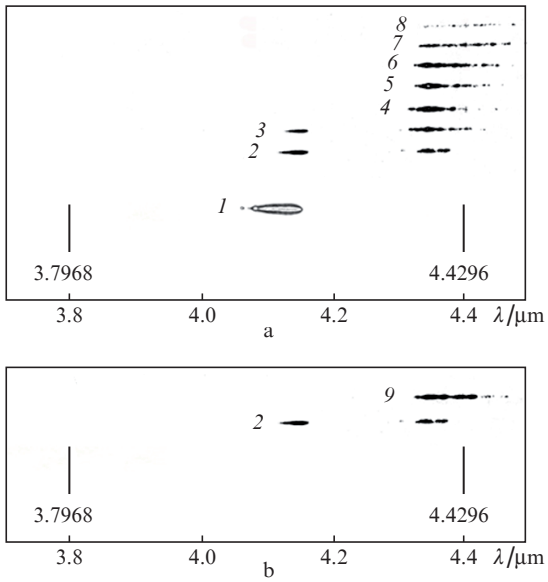

Figure 9. Lasing spectra of a Fe:ZnSe laser with active element 1 at ΔT = 100 K [(a), print (*1*)] and active element 2 at ΔT = 100 [(a), (*2*) and (b), (*2*)], 80 [(a), (*3*)], 60 [(a), (*4*)], 50 [(a), (*5*)], 40 [(a), (*6*)], 30 [(a), (*7*)], and 20 [(a), (*8*)] K in the single pump regime and in the steady repetitively pulsed regime at ν = 2 Hz and E_p = 6 J [(b), (*9*)]. The vertical bars indicate the positions of the 6th and 7th diffraction orders for the He–Ne laser line.

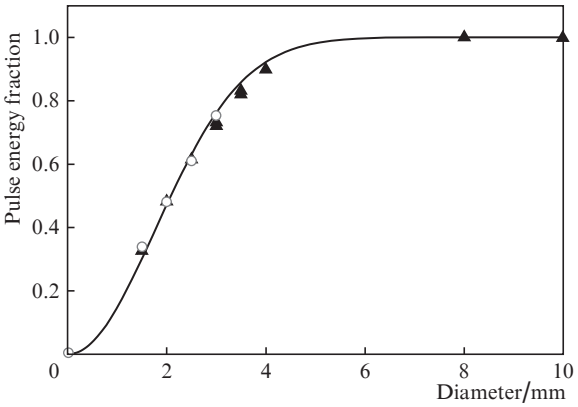

Figure 10. Dependence of the fraction of Fe:ZnSe laser pulse energy transmitted through a hole in the focal plane of a spherical mirror with a focal length of 500 mm on the hole diameter at a pump energy of 6.8 J in the (▲) single-pulse regime and (○) steady repetitively pulsed. The solid line is a similar dependence calculated for a beam with a transverse Gaussian intensity distribution and a radius w = 1.25 mm. The data were obtained using active element 2 and 350-μs pump pulses.

heating the crystal (when ΔT decreases), the lasing spectra become red-shifted.

The dependences of the fraction of the Fe:ZnSe laser pulse energy (at a pump energy of 6.8 J) transmitted through a diaphragm on the diaphragm diameter are presented in Fig. 10. Here, active element 2 and 350-μs pump pulses were used. The experimental data are described well by the transmission curve for a beam with a Gaussian intensity distribution and a radius w = 1.25 mm, transmitted through a hole with a diameter d. The total divergence angle of the laser beam was estimated as $\Theta = 2w/F$ = 5 mrad (F = 500 mm is the spherical mirror focal length). A 5-mrad angle contains ~65% energy. Note that the diameter of the fundamental TEM_{00} mode for the cavity in use can be estimated as

$$2w_0 = \sqrt{\frac{2L_c\lambda}{\pi}}\sqrt{\frac{R-L_c}{L_c}} = 1.5 \text{ mm},$$

where L_c is the cavity length and R is the curvature radius of the highly reflecting mirror. Then divergence of the fundamental Gaussian mode is $\Theta_0 = \lambda/(2\pi w_0)$ = 1 mrad. Thus, the measured divergence of the Fe:ZnSe laser beam exceeds the divergence of the TEM_{00} mode by a factor of about 5.

3.2. Laser characteristics in the repetitively pulsed pump regime

The first experiments on the application of this regime were performed for a pulse width of 700 μs using active element 1.

Figure 11 shows the dependence of the Fe:ZnSe laser pulse energy on the pulse serial number in a short series of 12 pulses with a repetition rate of 5 Hz. It can be seen that average radiation power in this series exceeded 20 W. During the first second of laser operation, we observed a significant rise in the output energy, which was followed by its slight decrease. This behaviour corresponds to the initial lasing dynamics of pump lasers operating in the repetitively pulsed regime (see Fig. 5a). Unfortunately, the pump lasers that were at our disposal could not reliably operate in the quasi-cw repetitively pulsed regime at ultimate pulse energies and frequencies of 5 Hz or higher.

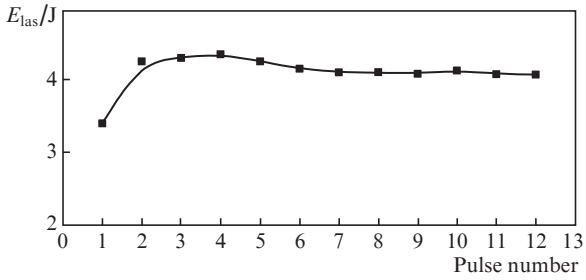

Figure 11. Dependence of the Fe:ZnSe laser pulse energy on the pulse serial number in a short series of 12 pulses at their repetition rate of 5 Hz and E_p = 12 J.

The time dependences of the average laser power in a series of 100 pulses at different pulse repetition rates are presented in Fig. 12. It can be seen that the average Fe:ZnSe laser power in a series of 100 pulses may reach ~10 W.

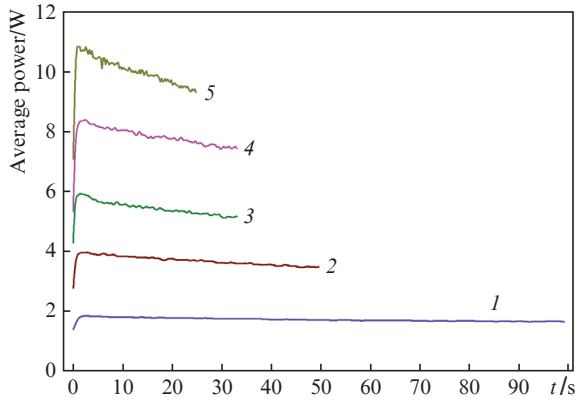

Figure 12. Time dependences of the average Fe:ZnSe laser power in a series of 100 pulses at different repetition rates and pump pulse energies: (*1*) 1 Hz, 5.9 J; (*2*) 2 Hz, 5.9 J; (*3*) 3 Hz, 5.9 J; (*4*) 3 Hz, 8.1 J; and (*5*) 4 Hz, 8.1 J.

Figure 13a shows a time dependence of the average Fe:ZnSe laser power in a series of more than 1500 pulses at a rate of 2 Hz. Here, we observed attainment of the steady-state operation regime of the repetitively pulsed laser 10–15 min after the operation onset; it was related to a change in the operation regime of thermoelectric modules. The maximum average Fe:ZnSe laser power was 2.8 W. The average power significantly decreases with an increase in the pulse repetition rate. It is demonstrated by Fig. 14, which presents the time dependences of the average laser power at approximately the same values of the average pump power. The decrease in the average power with an increase in the pulse rate is related to the less efficient operation of the pump laser (see Fig. 5), as well as with the more rapid drop of E_{las} upon crystal heating because of the small initial excess above the lasing threshold (see Fig. 7).

We related the possibility of increasing the average lasing power to a decrease in the pump pulse width. The time dependences of the average Fe:ZnSe laser power in the repetitively pulsed regime at a pump pulse repetition rate of 2 Hz, their width of 350 μs, and different energies are presented in Fig. 13b. The maximum average Fe:ZnSe laser power in the steady-

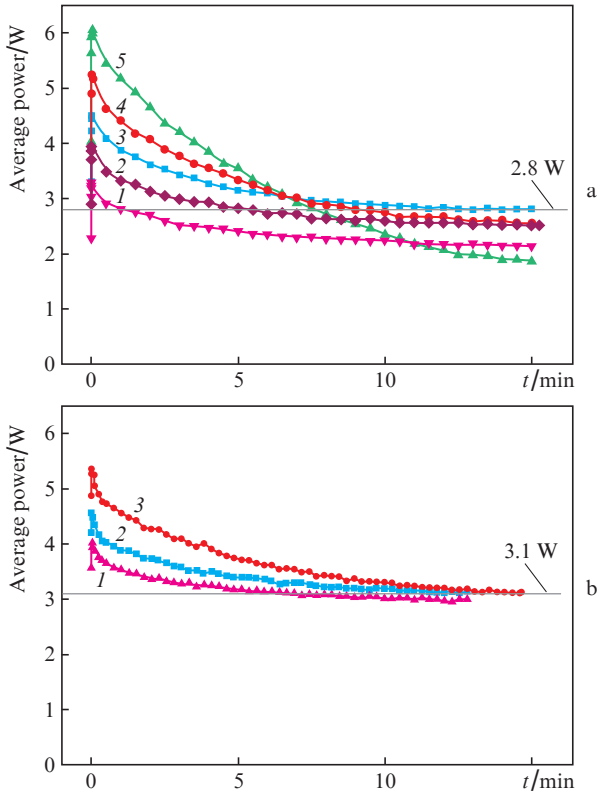

Figure 13. Time dependences of the average power of a Fe:ZnSe laser with active elements (a) 1 and (b) 2 in the repetitively pulsed pump regime at a pulse repetition rate of 2 Hz; pulse widths of (a) 700 and (b) 350 μs; and pump pulse energies of (*1*) 5, (*2*) 6, (*3*) 6.8, (*4*) 8.1, and (*5*) 9 J (a) and (*1*) 6, (*2*) 6.8, and (*3*) 8.1 J (b).

state repetitively pulsed regime was 3.1 W. Thus, shortening the pump pulse led to an increase in the laser power by about 10%.

The lasing spectrum of the Fe:ZnSe laser in the steady regime is presented in Fig. 9b as spectrum (*9*). It is significantly red-shifted with respect to the spectrum in the single-pulse pump regime and is peaking near $\lambda = 4.38$ μm at a width of 0.1 μm. The observed shift is due to the crystal heating, which leads to the broadening of the absorption band and a rise in the reabsorption of laser radiation in the long-wavelength edge of the absorption spectrum.

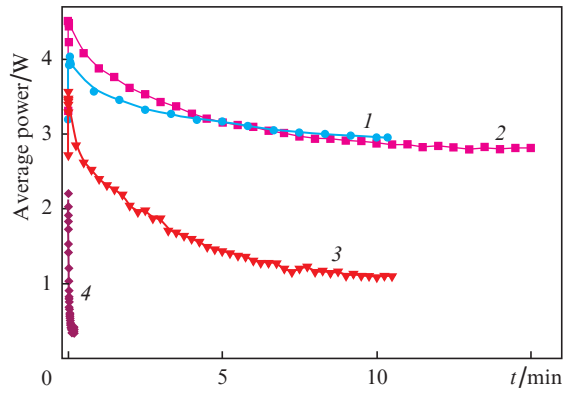

Figure 14. Time dependences of the average power of a Fe:ZnSe laser with active element 1 in the repetitively pulsed regime at approximately constant average pump power and pulse repetition rates of (*1*) 1.2, (*2*) 2, (*3*) 4, and (*4*) 10 Hz.

It can be seen in Fig. 10 that the radiation directivity of the Fe:ZnSe laser beam in the steady repetitively pulsed regime is practically the same as under the single pumping conditions.

4. Results and discussion

Prior to the laser operation onset, the active element, indium gaskets, and 'cold' plates of the thermoelectric module are cooled to a temperature of ~195 K. There is also some temperature distribution inside the thermoelectric modules. After switching on the laser in the repetitively pulsed pump regime, the active region is the first to be heated (adiabatic heating). Then the heat penetrates all previously cooled elements (heat removal is performed via equalisation of the temperatures of these elements with their specific heat involved). Finally, the system attains the steady regime as a result of changing the operation regime of thermoelectric modules so as to provide removal of supplied thermal pump power.

Let us first consider the removal of heat from the active region due to the heating of the neighbouring regions of the crystal. It follows from Fig. 7 that the pulse energy of the Fe:ZnSe laser decreases almost linearly with increasing crystal temperature, which is related to an increase in the lasing threshold (in the single-pulse pump regime the crystal temperature is equal to the temperature of the thermoelectric module 'cold' surface). This dependence can be written as

$$E_{las} = E_{0las} - \alpha \Delta \tilde{T} \tag{2a}$$

or

$$P_{las}^{av} = P_{0las}^{av} - \nu\alpha\Delta\tilde{T}, \tag{2b}$$

where $E_{0las} = kE_p$ and $P_{0las}^{av} = E_{0las}\nu$ are, respectively, the pulse energy and the average laser power at the minimum crystal temperature ($T = 195$ K); $\Delta\tilde{T}$ is the increment in the crystal temperature with respect to minimum; k is the laser efficiency; and α is the proportionality factor, which is equal to 0.03 J K^{-1} at $E_{0las} = 2.7$ J (see Fig. 7, upper curve). The factor k can be expressed in terms of the pump pulse threshold energy and the laser differential efficiency as $k = k_{dif}(1 - E_{th}/E_p)$, where $k_{dif} = 0.36$ and $E_{th} = 0.67$ J (see Fig. 6). Let us assume that the crystal is unlimited in the (x, y) plane, oriented perpendicular to the cavity optical axis. Active element 1 with large transverse sizes satisfies this assumption to a greater extent. Then the temperature increment $\Delta\tilde{T}$ can be written as [26]

$$\Delta\tilde{T}(x,y,t) = \int_0^t d\tau \int_{-r_0}^{r_0} d\varepsilon \int_{-\sqrt{(r_0^2-y^2)}}^{\sqrt{(r_0^2-y^2)}} d\delta \frac{E\nu F(\tau) R(\delta,\varepsilon)}{\pi r_0^2 l C}$$

$$\times \exp\left[-\frac{(x-\delta)^2 + (y-\varepsilon)^2}{4a^2(t-\tau)}\right][4a^2(t-\tau)]^{-1} =$$

$$= (E_p - E_{las})\nu f_\nu(x,y,t), \tag{3}$$

where $E = E_p - E_{las}$ is the part of the pump energy spent on crystal heating during one pulse; $r_0 = 0.4$ cm is the pump spot radius; $l = 1.7$ cm is the crystal length; $C = 1.6$ J cm^{-3} K^{-1} and $a^2 = 0.19$ cm^2 s^{-1} are, respectively, the volume specific heat and the thermal diffusivity of ZnSe crystal at $T \approx 200$ K; $F(t)$ is a time dependence, which can be written as the sum of a

sequence of δ functions, normalised to frequency; and $R(x, y)$ is the transverse intensity distribution in the pump beam, limited by the spot radius r_0 and similar to that measured in [23]. The heat release power is assumed to be the difference between the pump and laser powers. This simplification appears reasonable, because the luminescence quantum yield of the Fe:ZnSe crystal in the temperature range under consideration is much smaller than unity, and only a small fraction of the pump power is spent to excite luminescence.

A maximum increase in the crystal temperature occurs on the optical axis, where $x = y = 0$. Figure 15 shows the dependence $f_\nu(0, 0, t) = f_\nu(t)$. Dashed lines connect the points corresponding to the beginning of the pump pulse. This dependence will be denoted as $f_{0\nu}(t)$.

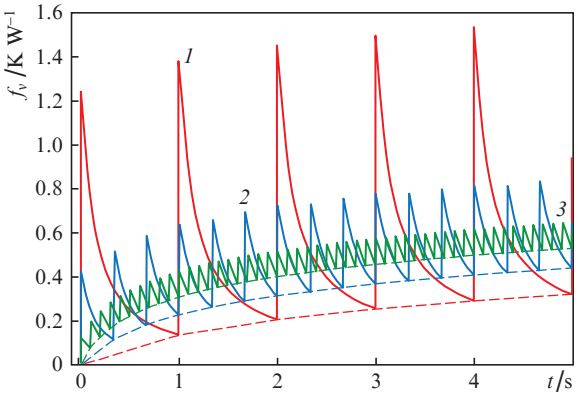

Figure 15. Dependences $f_\nu(t)$at ν = (*1*) 1, (*2*) 3, and (*3*) 10 Hz. The dashed line connecting the points corresponding to the pump pulse onsets are the dependences $f_{0\nu}(t)$.

Having replaced the function $f_\nu(x, y, t)$ with the function $f_{0\nu}(t)$ in the right-hand side of Eqn. (3), we obtain an expression for the increment in the crystal temperature up to the next pulse onset:

$$\Delta\tilde{T}(t) = (E_\mathrm{p} - E_\mathrm{las})\nu f_{0\nu}(t). \tag{4}$$

Then, substituting $\Delta\tilde{T}(t)$ into Eqn (2a) and solving its relative to E_las, we arrive at an expression for the average laser power $P_\mathrm{las}^\mathrm{av} = E_\mathrm{las}\nu$:

$$P_\mathrm{las}^\mathrm{av} = P_\mathrm{p}^\mathrm{av}[(k - \alpha\nu f_{0\nu}(t))/(1 - \alpha\nu f_{0\nu}(t))]. \tag{5}$$

It follows from formula (5) that, in the case of a short series of pump pulses, when $f_{0\nu}(t)$ is small (i.e., $k \gg \alpha\nu f_{0\nu}(t)$), the average laser power is approximately proportional to the pump power, and the laser efficiency is close to 36%. This situation corresponds to the data presented in Fig. 11 (the case where an average lasing power of 20 W, limiting for our system, was obtained during the first two seconds of laser operation).

For longer series of pump pulses, the laser power gradually decreases. In this case the heat reaches the crystal boundaries. However, formula (3) can be applied as previously if the change in the thermal diffusivity of material at crystal boundaries is taken into account. Calculations show that the consideration of this change does not affect much the increment in the temperature of the central part of active element 1 during the laser operation for 100 s.

If the pulse repetition rate is constant and the excess above the lasing threshold is sufficiently high (i.e., the dependence of the efficiency on E_p can be neglected), the average laser power is approximately proportional to the pump pulse energy. The time dependence of the power changes only slightly with a change in the pump pulse energy [Fig. 12; curves (*3*, *4*)]. At the same time, if the average pump power is maintained constant and the pulse repetition rate is increased, the average laser power rapidly decreases, which is in qualitative agreement with the dependences presented in Fig. 14. This decrease is explained as follows: to maintain the pump power constant with an increase in frequency, one must reduce the pulse energy, as a result of which the excess above the lasing threshold decreases.

Let us now estimate the average laser power under steady-state conditions. The dependence of the thermal power that can be removed by two thermoelectric modules on the temperature difference on these modules is given by the formula

$$Q = \beta\Delta T_\mathrm{TM}, \tag{6}$$

where β is a proportionality factor, equal to 0.34 W K^{-1} for the thermoelectric modules used by us, and ΔT_TM is the temperature difference between the extremely low temperature of the 'cold' surface of the thermoelectric module and the temperature of the same surface under conditions of steady repetitively pulsed pumping. The ΔT_TM value is smaller than $\Delta\tilde{T}$, because there is also a temperature difference between the centre of the crystal active region and the 'cold' surface of the thermoelectric module in the steady regime:

$$\Delta T_\mathrm{TM} = \delta\Delta\tilde{T}. \tag{7}$$

Then, rewriting Eqn (6) with allowance for (7) and (2b) and equating Q to $P_\mathrm{p}^\mathrm{av} - P_\mathrm{las}^\mathrm{av}$, we arrive at the expression for the average laser power in the steady regime:

$$P_\mathrm{las}^\mathrm{av} = P_\mathrm{p}^\mathrm{av}\left[\frac{k - \alpha\nu/(\beta\delta)}{1 - \alpha\nu/(\beta\delta)}\right]. \tag{8}$$

As an example, we will consider the case corresponding to curve (*3*) in Fig. 13b: P_p^av = 16.2 W, k = 0.34 (see Fig. 6, for E_p = 8.1 J), α = 0.03 J K^{-1}, ν = 2 s^{-1}, and β = 0.34 W K^{-1}. The factor δ in (7) can be estimated proceeding from the following considerations. Having substituted the experimentally measured value $P_\mathrm{las}^\mathrm{av}$ = 3.1 W into Eqn (2b), we find that $\Delta\tilde{T}$ = 40 K. Let us now estimate the temperature difference implemented in the cylindrical active element clamped in a copper holder. To this end, one must solve the steady-state heat conduction equation in cylindrical coordinates. On the assumption that the power of homogeneous heat release in the central region of active element with a radius r_0 = 0.4 cm is $P_\mathrm{p}^\mathrm{av} - P_\mathrm{las}^\mathrm{av} \approx$ 13.1 W and that the temperature on the lateral surface of cylindrical active element of radius R_0 = 0.6 cm is maintained constant, it can easily be shown that the temperature difference between the cylinder centre and lateral surface is determined by the formula

$$\Delta T_\mathrm{c} = \frac{P_\mathrm{p}^\mathrm{av} - P_\mathrm{las}^\mathrm{av}}{2\pi l\chi}\left[0.5 + \ln\left(\frac{R_0}{r_0}\right)\right], \tag{9}$$

where l = 1.93 cm is the length of active element 2 and χ = 0.23 W cm^{-1} K^{-1} is the thermal conductivity of ZnSe at a tem-

perature of 200 K. Formula (9) yields $\Delta T_c \approx 4$ K. Furthermore, using formula (7) and taking into account that $\Delta T_{TM} = \Delta \tilde{T} - \Delta T_c$, we obtain the following estimate: $\delta \approx 0.9$. Then, we find from formula (8) that $P_{las}^{av} = 2.9$ W, which almost coincides with the measured value of 3.1 W.

5. Conclusions

We presented a repetitively pulsed Fe:ZnSe laser, which has an active crystal cooled by two four-cascade thermoelectric modules and is pumped by two Er:YAG lasers. An average laser power of 20 W was obtained for 2 s in the unstable regime, whereas the average power under steady-state conditions turned out to be 3.1 W at a pump pulse repetition rate of 2 Hz and a pulse width of 350 s. The lasing spectrum was peaking near $\lambda = 4.38$ μm. The laser beam was axisymmetric, and the cone with an angle of 5 mrad contained 65% of the Fe:ZnSe laser power. The experimental values of average lasing power are in good agreement with the calculation results. The average laser power is determined to a great extent by the characteristics of the thermoelectric modules.

Acknowledgements. This work was supported by the Presidium of the Russian Academy of Sciences (Urgent Problems of Photonics and Sensing of Inhomogeneous Media and Materials Programme No. 7) and (in part) by the Programme for Increasing the Competitiveness of the National Research Nuclear University 'MEPhI' (Contract No. 02.a03.21.0005).

References

1. Akimov V.A., Kozlovsky V.I., Korostelin Yu.V., Landman A.I., Podmar'kov Yu.P., Frolov M.P. *Quantum Electron.*, **34**, 185 (2004) [*Kvantovaya Elektron.*, **34**, 185 (2004)].
2. Picque N., Gueye F., Guelachvili G., Sorokin E., Sorokina I.T. *Opt. Lett.*, **30** (24), 3410 (2005).
3. Akimov V.A., Kozlovsky V.I., Korostelin Yu.V., Landman A.I., Podmar'kov Yu.P., Frolov M.P. *Quantum Electron.*, **35**, 425 (2005) [*Kvantovaya Elektron.*, **35**, 425 (2005)].
4. Herbin H., Picque N., Guelachvili G., Sorokin E., Sorokina I.T. *J. Mol. Spectrosc.*, **238**, 256 (2006).
5. Girard V., Farrenq R., Sorokin E., Sorokina I.T., Guelachvili G., Picque N. *Chem. Phys. Lett.*, **419**, 584 (2006).
6. Sorokin E., Sorokina I.T., Mandon J., Guelachvili G., Picque N. *Opt. Express*, **15**, 16540 (2007).
7. Akimov V.A., Voronov A.A., Kozlovsky V.I., Korostelin Yu.V., Landman A.I., Podmar'kov Yu.P., Frolov M.P. *Quantum Electron.*, **37**, 1071 (2007) [*Kvantovaya Elektron.*, **37**, 1071 (2007)].
8. Kozlovsky V.I., Korostelin Yu.V., Okhotnikov O.G., Podmar'kov Yu.P., Skasyrsky Ya.K., Frolov M.P., Akimov V.A. *Quantum Electron.*, **43**, 885 (2013) [*Kvantovaya Elektron.*, **43**, 885 (2013)].
9. Gubin M.A., Kireev A.N., Korostelin Yu.V., Landman A.I., Podmar'kov Yu.P., Filipchuk M.Yu., Frolov M.P., Shelkovnikov A.I. *Kratk. Soobshch. Fiz. FIAN*, **38**, 34 (2011).
10. Gubin M.A., Kireev A.N., Korostelin Yu.V., Landman A.I., Pnev A.B., Podmar'kov Yu.P., Filipchuk M.Yu., Frolov M.P., Shelestov D.A., Shelkovnikov A.S. *Quantum Electron.*, **42**, 509 (2012) [*Kvantovaya Elektron.*, **42**, 509 (2012)].
11. Gubin M.A., Kireev A.N., Kozlovsky V.I., Korostelin Yu.V., Lazarev V.A., Pnev A.B., Podmar'kov Yu.P., Tyurikov D.A., Frolov M.P., Shelkovnikov A.S. *Quantum Electron.*, **42**, 565 (2012) [*Kvantovaya Elektron.*, **42**, 565 (2012)].
12. Sorokin E., Tolstik N., Sorokina I.T. *Proc. SPIE*, **8599**, 859916 (2013).
13. Sorokina I.T., Sorokin E. *IEEE J. Sel. Top. Quantum Electron.*, **21**, 1601519 (2015).
14. Vasilyev S., Mirov M., Gapontsev V. *Opt. Express*, **22**, 5118 (2014).
15. Potemkin F.V., Migal E.A., Pushkin A.V., Sirotkin A.A., Kozlovsky V.I., Korostelin Y.V., Podmar'kov Y.P., Firsov V.V., Frolov M.P., Gordienko V.M. *Laser Phys. Lett.*, **13**, 125403 (2016).
16. Potemkin F.V., Bravy B.G., Kozlovsky V.I., Korostelin Y.V., Migal E.A., Podmar'kov Y.P., Podshivalov A.A., Platonenko V.T., Firsov V.V., Frolov M.P., Gordienko V.M. *Laser Phys. Lett.*, **13**, 15401 (2016).
17. Bravyi B.G., Gordienko V.M., Kozlovsky V.I., Korostelin Yu.V., Potemkin F.V., Podmar'kov Yu.P., Podshivalov A.A., Platonenko V.T., Firsov V.V., Frolov M.P. *Izv. RAN, Ser. Fiz.*, **80**, 489 (2016).
18. Potemkin F.V., Migal E.A., Pushkin A.V., Bravy B.G., Sirotkin A.A., Kozlovsky V.I., Korostelin Yu.V., Podmar'kov Yu.P., Firsov V.V., Frolov M.P., Gordienko V.M. *Proc. SPIE*, **10238**, 102380L (2017).
19. Kozlovsky V.I., Korostelin Y.V., Podmar'kov Y.P., Skasyrsky Y.K., Frolov M.P. *J. Phys.: Conf. Ser.*, **740**, 012006 (2016).
20. Mirov S., Fedorov V., Martyshkin D., Moskalev I., Mirov M., Vasilyev S., in *Advanced Solid State Lasers Conf. 2015* (OSA, 2015) paper AW4A.
21. Velikanov S.D., Gavrishchuk E.M., Zaretskii N.A., Zakhryapa A.V., Ikonnikov V.B., Kazantsev S.Yu., Kononov I.G., Maneshkin A.A., Mashkovskii D.A., Saltykov E.V., Firsov K.N., Chuvatkin R.S., Yutkin I.M. *Quantum Electron.*, **47**, 303 (2017) [*Kvantovaya Elektron.*, **47**, 303 (2017)].
22. Voronov A.A., Kozlovsky V.I., Korostelin Yu.V., Landman A.I., Podmar'kov Yu.P., Frolov M.P. *Quantum Electron.*, **35**, 809 (2005) [*Kvantovaya Elektron.*, **35**, 809 (2005)].
23. Frolov M.P., Korostelin Yu.V., Kozlovsky V.I., Podmar'kov Yu.P., Skasyrsky Ya.K. *Opt. Lett.*, **43**, 623 (2018).
24. Kozlovsky V.I., Akimov V.A., Frolov M.P., Korostelin Yu.V., Landman A.I., Martovitsky V.P., Mislavskii V.V., Podmar'kov Yu.P., Skasyrsky Ya.K., Voronov A.A. *Phys. Stat. Sol. B*, **247**, 1553 (2010).
25. Moulton P.F. *IEEE J. Quantum Electron.*, **21**, 1582 (1985).
26. Vladimirov V.S. *Uravneniya matematicheskoi fiziki* (Equations of Mathematical Physics) (Moscow: Nauka, 1971) p. 258.